JACS
JOURNAL OF THE AMERICAN CHEMICAL SOCIETY
Article
pubs.acs.org/JACS

Magnetoluminescent Light Switches – Dual Modality in DNA Detection

Eric D. Smolensky, Katie L. Peterson, Evan A. Weitz, Cutler Lewandowski, and Valérie C. Pierre*

Department of Chemistry, University of Minnesota, Minneapolis, Minnesota 55455, United States

ABSTRACT: The synthesis and properties of two responsive magnetoluminescent iron oxide nanoparticles for dual detection of DNA by MRI and luminescence spectroscopy are presented. These magnetoluminescent agents consist of iron oxide nanoparticles conjugated with metallointercalators via a polyethylene glycol linker. Two metallointercalators were investigated: Ru(bpy′)(phen)(dppz), which turns on upon DNA intercalation, and Eu-DOTA-Phen, which turns off. The characteristic light-switch responses of the metallointercalators are not affected by the iron oxide nanoparticles; upon binding to DNA the luminescence of the ruthenium complexes increases by ca. 20-fold, whereas that of the europium complex is >95% quenched. Additionally, the 17−20 nm magnetite cores, having permeable PEG coatings and stable dopamide anchors, render the two constructs efficient responsive contrast agents for MRI with unbound longitudinal and transverse relaxivities of 12.4−9.2 and 135−128 $mM^{-1}{}_{Fe}s^{-1}$, respectively. Intercalation of the metal complexes in DNA results in the formation of large clusters of nanoparticles with a resultant decrease of both r_1 and r_2 by 32−63% and 24−38%, respectively. The potential application of these responsive magnetoluminescent assemblies and their reversible catch-and-release properties for the purification of DNA is presented.

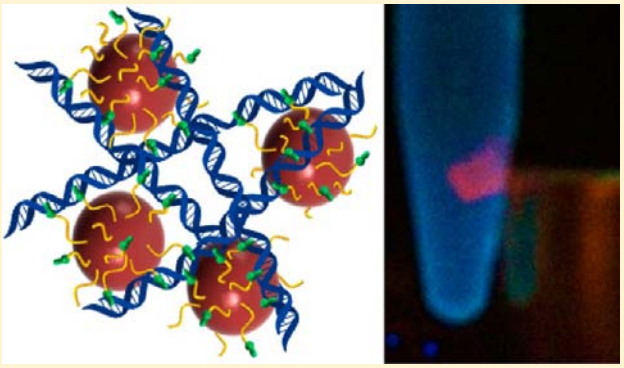

INTRODUCTION

Multimodal nanocomposite probes—nanoparticle assemblies that enable imaging by two or more techniques—have become increasingly prevalent over the past decade. Of these, magnetoluminescent[1−8] and magnetoplasmonic[9,10] agents are receiving the most attention due to their ability to combine two widespread techniques, magnetic resonance imaging (MRI) and confocal or dark-field microscopy, which are complementary in terms of three-dimensional imaging capability and spatial resolution, respectively. Particulate magnetoluminescent probes are most often composed of superparamagnetic metallic nanoparticles, preferentially magnetite or maghemite, which confers to the assembly the high transverse relaxivity necessary for MRI. The metallic crystals are either directly functionalized with luminescent dyes, or the dyes are embedded in a surrounding silica matrix. Organic dyes are employed most commonly in these assemblies due to their commercial availability and high quantum yield. More recently, complexes of ruthenium[11−14] and luminescent lanthanides (terbium and europium)[15,16] have also been reported. These offer the notable advantage of long luminescence lifetimes that enable time-gated detection and thus improved sensitivity in complex biological media. More importantly, their large Stokes shifts also minimize intrananoparticle luminescence quenching. This is particularly beneficial as recent studies by Simard have indicated that decreased luminescence of magnetoluminescent assemblies containing organic dyes is not due to quenching from the iron oxide nanoparticles but to aggregation of the dyes in the silica matrix.[17] This quenching is substantially reduced with the use of dyes with long luminescence lifetimes, such as the ruthenium and lanthanide complexes used herein. Although the design and behavior of magnetoluminescent probes are increasingly understood, all current work has so far focused on nonresponsive probes that do not report on the presence or absence of specific, targeted biomarkers. Aside from our recent example of a dual-responsive magnetoplasmonic assembly,[18] no dual responsive multimodal nanoparticle has yet been reported. Yet, as the increasing number of publications on particulate-responsive MRI contrast agents indicates, such probes are particularly sought after by the biomedical community. Herein we report the synthesis and evaluation of two responsive magnetoluminescent nanocomposites that detect dsDNA by MRI, as determined by a change in longitudinal and transverse relaxivities and by luminescence.

The responsive magnetoluminescent probes, Fe_3O_4@Dop-PEG-Eu-DOTA-Phen (**1**) and Fe_3O_4@Dop-PEG-Ru(bpy′)-(phen)(dppz) (**2**), consist of a magnetite core with high saturation magnetization functionalized with either a lanthanide or a ruthenium metallointercalator bound to the iron oxide surface via a stable dopamide anchor (Figure 1).[19] Both metallointercalators behave as DNA light switches. The time-gated luminescence of europium and terbium complexes of DOTA-Phen is quenched >95% upon intercalation of the phenanthridine antenna in the DNA base stack. This observation correlates to photoelectron transfer of guanosine

Received: February 27, 2013
Published: May 21, 2013

   dx.doi.org/10.1021/ja402107x | J. Am. Chem. Soc. 2013, 135, 8966−8972

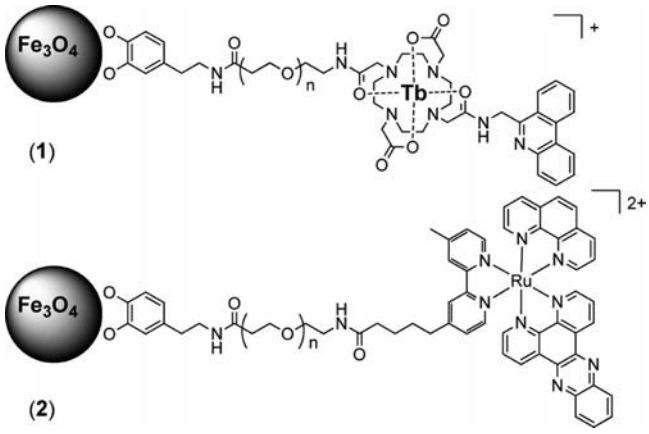

Figure 1. Chemical structure of the dual responsive magnetolight switches, **1** and **2**.

and, to a lesser extent, adenosine, to the phenanthridine.[20−25] As a result **1** is expected to behave as a turn-off magnetic light switch. On the other hand, the luminescence of the ruthenium dppz complex in aqueous solution increases over 10-fold upon intercalation in the major groove of dsDNA,[26−34] such that **2** was designed as a turn-on light switch. Importantly, both magnetoluminescent probes were also designed to behave as responsive MRI contrast agents. Intercalation of the phenanthridine and dppz ligands of **1** and **2** in the base stack of DNA, respectively, was anticipated to create three-dimensional arrays of nanoparticles intermingled with DNA (Figure 2). Such

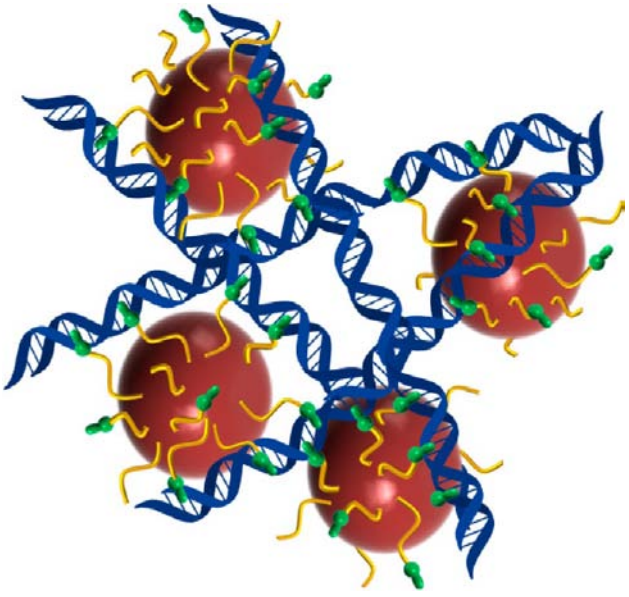

Figure 2. Principle of action of the dual responsive magnetolight switches. Intercalation of the Phen and dppz ligands in DNA causes the europium and ruthenium complex to turn off and on, respectively. Intercalation also causes aggregation of the iron oxide nanoparticles which decreases both their r_1 and r_2.

aggregation is known to affect both the longitudinal and the transverse relaxivity of superparamagnetic iron oxide nanoparticles and is the basis for responsive particulate MRI contrast agents.[35−41] As such, the response of both probes to DNA was expected to be observable not only by luminescence but also by MRI.

RESULTS AND DISCUSSION

Synthesis and Characterization of the Magnetoluminescent Assemblies. The two bimetallic nanocomposites were synthesized from a common intermediate, Fe_3O_4@Dop-PEG-NH_2 (**4**, Scheme 1), which was obtained by

Scheme 1. Synthesis of 1 and 2[a]

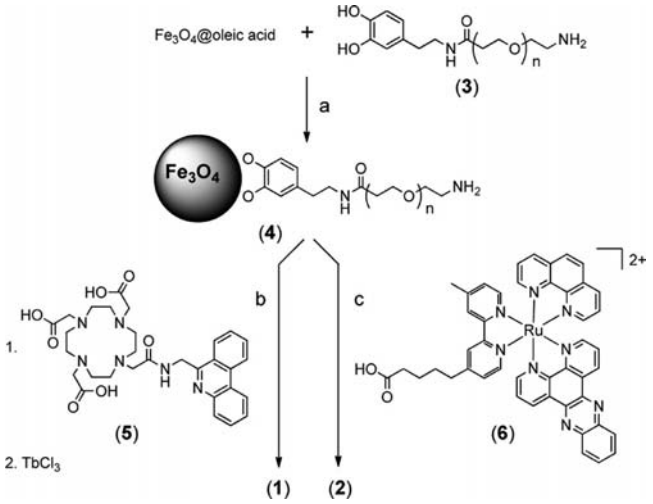

[a]Reagents and conditions: (a) hexanes/H_2O pH 14, rt, 12 h; (b) i. DOTA-Phen, EDC, NHS, NEt_3, rt, 8 h; ii. $EuCl_3$, H_2O, pH 7, 40 °C, 60 h; (c) EDC, NHS, NEt_3, rt, 15 h.

refunctionalizing oleic acid coated magnetite nanoparticles with a catechol-terminated polymer according to a biphasic procedure previously reported.[19] The peripheral amines of the nanoparticles were then conjugated either to the macrocyclic ligand DOTA-Phen (**5**) or to the acid-functionalized Ru(bpy′)-(phen)(dppz) using standard amide coupling conditions. The syntheses of Fe_3O_4@oleic acid nanoparticles,[42] the catechol-terminated polymer Dop-PEG-NH_2 (**3**),[41] the macrocyclic ligand DOTA-Phen (**5**),[20,25] and the ruthenium intercalating complex, Ru(bpy′)(phen)(dppz) (**6**)[26,43−45] were performed as previously reported. The iron/lanthanide composite is then obtained by heating the DOTA-Phen coated nanoparticles at 40 °C with an excess of $EuCl_3$ at neutral pH. The efficacy of the conjugation was established by ICP-MS in terms of Fe:Eu and Fe:Ru ratio, respectively, and by infrared spectroscopy (Figure 3). TEM (Figure 4) confirmed that the size of the nanoparticles was not affected by the reactions. The Fe:Eu and Fe:Ru assemblies were 17.8 ± 1.4 and 20.4 ± 1.6 nm in diameter, respectively. This size was selected as it is the optimum size to achieve maximum longitudinal and transverse relaxivities.[46]

Although it should be assumed that not all peripheral amines on the nanoparticles have been conjugated to the intercalators, the high Fe:Eu ratio of 67:60 suggests a very effective reaction with the DOTA-Phen ligand. On the other hand, the low Fe:Ru ratio of 87:1 highlights a much less efficient conjugation with the bulkier ruthenium complex which, unfortunately, we were not able to improve by varying reaction conditions. One advantage of this synthetic approach concerns the Fe/Eu nanoparticles. This core−shell assembly is composed of two hard metals. Our initial attempts to directly functionalize the nanoparticles with the polymer−lanthanide complex, Dop-PEG-Eu-DOTA-Phen, were unsuccessful. The high affinity of the catechol anchor for the lanthanides prevented efficient functionalization of the iron oxide crystals.[19] Predictably, direct

dx.doi.org/10.1021/ja402107x | J. Am. Chem. Soc. 2013, 135, 8966−8972

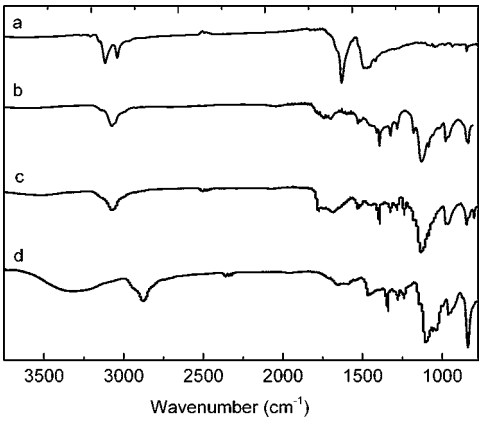

Figure 3. Infrared spectra of (a) Fe_3O_4@oleic acid, (b) **4**, (c) **1**, and (d) **2**.

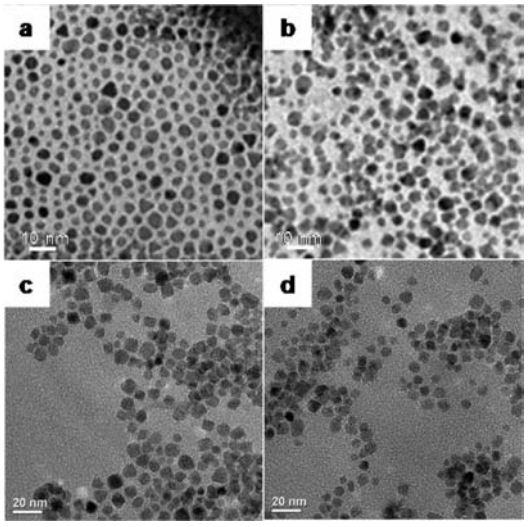

Figure 4. Transmission electron micrographs of (a) MION@OA, (b) MION@DPEGNH$_2$, (c) **1**, and (d) **2**.

conjugation of the europium complex, Eu-DOTA-Phen, to the amine coated nanoparticles, Fe_3O_4@Dop-PEG-NH_2, also failed; the carboxylate arms of the macrocycle are unreactive when coordinated to the lanthanide ion. The three-step synthesis of the Fe/Eu nanocomposite described above was the highest yielding synthetic route.

Light Switch Response. Both the europium and ruthenium coated nanoparticles were designed to behave as luminescent light switches for DNA detection, albeit with opposite responses. The phenanthridine antenna of the europium complex is a known intercalate in dsDNA.[21−24] This intercalation quenches both the fluorescence of the antenna and the phosphorescence of the lanthanide. Our group and Parker's have previously demonstrated that this quenching likely occurs via photoelectron transfer from the purine base guanosine and to a lesser extent adenosine to the phenanthridine antenna.[21−24] As predicted, addition of CT DNA or any dsDNA oligonucleotide to the Fe/Eu nanocomposites efficiently quenches lanthanide-centered time-gated luminescence (Figures 5). This quenching is more pronounced at lower excitation wavelengths where PeT is favored: 99% of the phosphorescence is quenched upon excitation at 254 nm, whereas only 35% is quenched with $\lambda_{excitation}$ = 347 nm (Figure 6). Advantageously, at the short wavelength of widespread

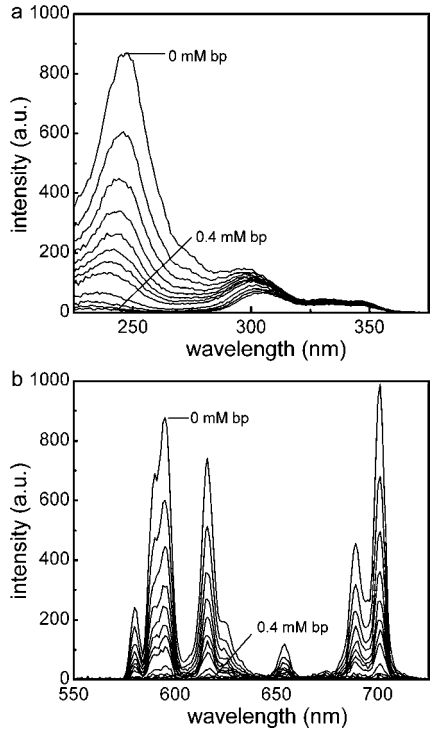

Figure 5. Time-gated (a) excitation and (b) emission spectra of **1** upon addition of increasing concentrations of CT DNA. Experimental conditions: PBS, pH 7.4, $[Fe]_{total}$ = 11 μM, $[Eu]_{total}$ = 9.8 μM, T = 20 °C, time delay = 0.1 ms, (a) $\lambda_{emission}$ = 615 nm, (b) $\lambda_{excitation}$ = 254 nm.

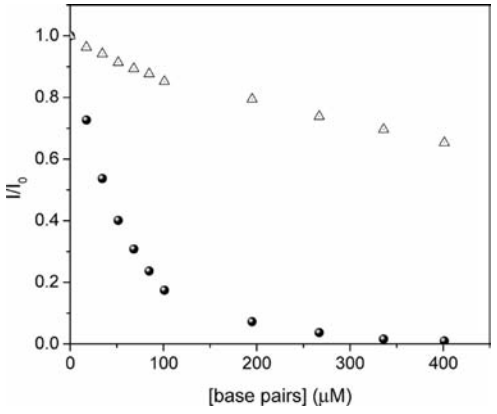

Figure 6. Decrease in time-gated luminescence intensity of **1** upon addition of CT DNA base pairs upon excitation a $\lambda_{excitation}$ = 254 nm (solid circles, ●) and 347 nm (open triangles, △. Experimental conditions: PBS, pH 7.4, $[Fe]_{total}$ = 11 μM, $[Eu]_{total}$ = 9.8 μM, T = 20 °C, time delay = 0.1 ms, integrated emission between λ = 550−750 nm.

portable UV lamps, the substantial quenching is readily observable with the naked eye (Figure 7). The ruthenium analog, **2**, on the other hand, was designed as a turn-on magnetolight switch (Figure 8). Unfortunately, poor conjugation of the ruthenium complex on the nanoparticles led to mediocre turn-on activity upon addition of calf-thymus DNA, although it is still noticeable with the naked eye (Figure 9). Notably, the response observed upon intercalation in dsDNA is comparable to that reported by Barton for the parent $Ru(bpy)_2(dppz)$.[26] Notably, the light-switch responses observed for Eu-DOTA-Phen (turn-off) and $Ru(bpy)_2(dppz)$ (turn-on) occurs only upon intercalation in dsDNA. Mere

dx.doi.org/10.1021/ja402107x | J. Am. Chem. Soc. 2013, 135, 8966−8972

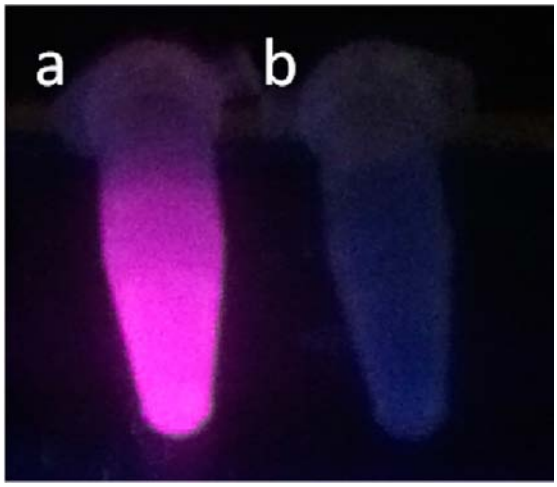

Figure 7. Luminescence of **1** upon excitation with a portable UV lamp in the (a) absence and (b) presence of CT DNA. Experimental conditions: PBS, pH 7.4, T = 20 °C, $\lambda_{excitation}$ = 254 nm.

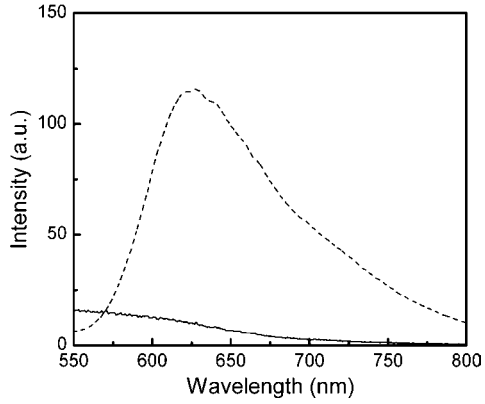

Figure 8. Luminescence of Ru(bpy′)(phen)(dppz) in the absence (solid line) and presence (dotted line) of CT DNA. Experimental conditions: PBS, pH 7.4, $\lambda_{excitation}$ = 482 nm, T = 20 °C.

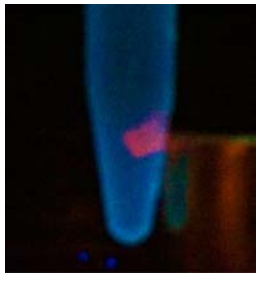

Figure 9. Luminescence of **2** in the presence of CT DNA upon excitation with a portable UV lamp. The **2**·DNA cluster is readily and reversibly separated with a rare earth magnet. Experimental conditions: PBS/ethanol, pH 7.4, $\lambda_{excitation}$ = 254 nm, T = 20 °C.

interactions with single stranded oligonucleotides are not sufficient to yield the same light-switch response. Compared to dsDNA, addition of ssDNA at the same concentration of bases does not noticeably impact the luminescence of either Ru(bpy′)(phen)(dppz) or Eu-DOTA-Phen. Note that ssDNA can quench Eu-DOTA-Phen's luminescence but only at concentrations that are substantially higher than that needed with dsDNA, i.e., >20 mM bases for ssDNA versus 50 μM for dsDNA.

Relaxivity Response. Intercalation of the phenanthridine (Phen) or dipyrido[3,2-a:2′,3′-c]phenazine (dppz) ligands in dsDNA results in three-dimensional networks of nanoparticles intertwined with DNA (Figure 2). The formation of this network affects both their longitudinal (r_1) and transverse (r_2) relaxivities. In terms of longitudinal relaxivity, addition of DNA to the Fe/Eu (**1**) and Fe/Ru (**2**) nanocomposites decreases r_1 by 33% and 61% (Figures 10 and 11, respectively). This result

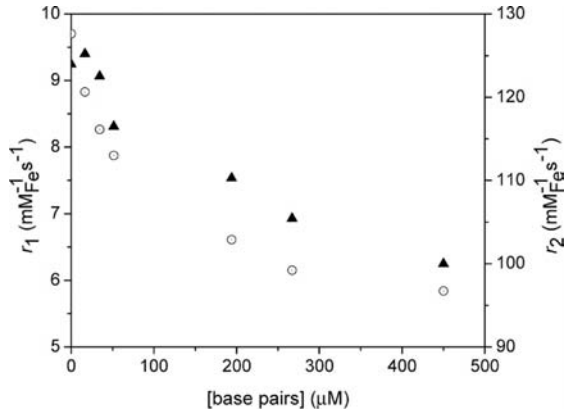

Figure 10. Decrease in longitudinal (r_1, ▲) and transverse (r_2, ○) relaxivities of **1** upon addition of CT DNA. Experimental conditions: PBS, pH 7.4, 1.5 T (60 MHz), T = 37 °C.

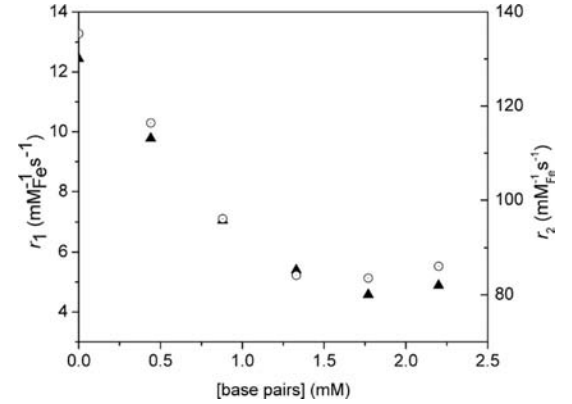

Figure 11. Decrease in longitudinal (r_1, ▲) and transverse (r_2, ○) relaxivities of **2** upon addition of CT DNA. Experimental conditions: PBS, pH 7.4, 1.5 T (60 MHz), T = 37 °C.

is consistent with prior observations from our group[41] and others[47,48] and is likely due to the formation of two pools of water that exchange significantly slower than the NMR time scale. The water trapped within the network relaxes rapidly due to its proximity to multiple iron oxide nanoparticles. This fast-relaxing water pool is, however, negligible compared to the bulk water that resides outside of the array and which is little affected by the DNA/nanoparticle cluster. Since the water between the two pools exchange slowly, the overall result is a decrease in r_1.

Interestingly, the transverse relaxivity, r_2, also decreases upon addition of DNA for both nanocomposites. This observation appears to be contradictory to that of previous responsive particulate contrast agents. It is, however, predictable given the size of the networks formed. Unlike for longitudinal relaxation, the effects observed for transverse relaxivity arise from changes in the global structure of the cluster and the magnetic field

dx.doi.org/10.1021/ja402107x | J. Am. Chem. Soc. 2013, 135, 8966−8972

surrounding it. As demonstrated by Gillis[47,48] and ourselves,[41] increase in transverse relaxivity with clustering of nanoparticles is only observed for small substrates and, most importantly, small clusters that maintain the motional averaging condition.[47,48] In these cases, the cluster itself behaves as a large magnetized sphere whose total magnetic moment increases according to Langevin's law. The relaxation is governed by the outer-sphere relaxation theory and is characterized by a long correlation time. In our case, however, the long length of CT DNA leads immediately to the formation of very large nanoparticle/DNA clusters. The motional averaging condition breaks down; r_2 is instead governed by the static dephasing regime. The translational diffusion time of a proton across the cluster is slowed enough such that its motion, relative to the cluster, is static. Consequently, as the concentration of DNA increases, r_2 decreases further with increasing cluster size. Note that the relaxivities of the "bare" nanoparticles which are not functionalized with either metallointercalators, **4**, actually increase slightly upon addition of dsDNA. This response is opposite to that observed when the nanoparticles are coated with metallointercalators thereby supporting our assertion that the decrease in relaxivities observed for the magnetolight switches **1** and **2** results from intercalation of the metal complex in dsDNA.

Catch-and-Release of DNA. The combination of superparamagnetic iron oxide nanoparticles with light-switch metallointercalators that bind reversibly to dsDNA opens the intriguing possibility of using the nanocomposites for catch-and-release separation and purification of DNA (Figure 12).

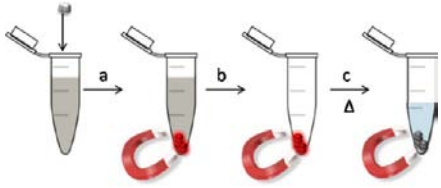

Figure 12. Catch-and-release purification of DNA with **2**: (a) The nanoparticles are added to a mixture containing DNA; upon intercalation in DNA, the luminescence of the nanoparticles is switched on. (b) The clusters of nanoparticles with DNA are magnetically separated from the rest of the mixture. Addition of PBS buffer and gentle heating to 80 °C releases the DNA from the nanoparticles, and the unbound nanoparticles are then separated magnetically from the hot suspension.

Addition of either **1** or **2** to a mixture containing DNA aggregates the polynucleotide with the nanoparticles. The presence of the DNA is at first monitored from the turn-on or turn-off light-switch behavior of the metallointercalator upon UV excitation. For instance, Fe_3O_4@Dop-PEG-Eu-DOTA-Phen is brightly luminescent in water (Figure 13a). Addition of a dispersion of these nanoparticles to a buffered solution containing dsDNA quenches the lanthanide luminescence (Figure 13b,c). In this case, nanoparticles were added until some luminescence reappeared so as to ensure that all DNA was caught. At this point, the DNA/nanocomposite clusters can readily be separated from the rest of the mixture with a small rare-earth magnet (Figure 13d). Note that in the case of the ruthenium functionalized iron oxide nanoparticles (**2**), this is best observed under UV (Figure 9). At this point, the supernatant which does not contain DNA can be readily pipetted off. The nanoparticles/DNA clusters were redispersed

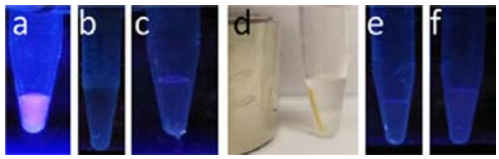

Figure 13. (a) A dispersion of Fe_3O_4@Dop-PEG-Eu-DOTA-Phen in water is luminescent, while (b) a solution of dsDNA in PBS buffer is not. (c) Addition of the magnetoluminescent nanoparticles to DNA results in extended nucleotide/nanoparticle networks which are no longer luminescent but (d) can be readily separated from the rest of the aqueous solution with a magnet. Heating the nanoparticles in water releases both the DNA and the metallointercalators such that neither the nanoparticles redispersed in water (e) nor the supernatant redisolved in water (f) are luminescent.

in water and heated past the oligonucleotide melting point to release the DNA. Note that, unfortunately, the catecholamide linker used to anchor the pegylated metallointercalators is not stable enough at high temperature, such that the Dop-PEG-Eu-DOTA-Phen was released with the DNA. Although the iron oxide nanoparticles could readily be removed magnetically, DNA could only be obtained with the metallointercalators. We are currently investigating a more stable anchor to alleviate this problem and increase the efficiency of catch-and-release purification.

CONCLUSION

Iron oxide nanoparticles functionalized with light-switch DNA metallointercalators behave as efficient probes with dual response by both luminescence and relaxivity. The luminescence response is a function of the metallointercalator. Ru(bpy′)(phen)(dppz) function as a turn-on light switch upon intercalation in the DNA helix whereas the lanthanide complex, Eu-DOTA-Phen, behaves as an efficient turn-off switch. The response of either intercalator is not affected by the iron oxide nanoparticle. Intercalation of the metal complexes in the DNA helix creates three-dimensional clusters that affect both the longitudinal and transverse relaxivities of the assembly. Regardless of the metallointercalator coating, coclustering with DNA results in a decrease of both r_1 and r_2. These decreases are due to the slow exchange of the water molecules trapped inside the cluster with outside bulk solvent and to the very slow translational diffusion time of protons across the cluster, such that the nanoparticles stay in a static dephasing regime. The combination of the two responses and the reversibility in the intercalation opens the possibility to use the magnetoplasmonic light switches for catch-and-release purification of DNA.

METHODS

General Considerations. Unless otherwise noted, starting materials were obtained from commercial suppliers and used without further purification. Water was distilled and further purified by a Millipore cartridge system (resistivity 18 MΩ). ^{1}H NMR and ^{13}C NMR spectra were recorded on a Varian 300 at 300 and 75 MHz or on a Varian 500 at 500 and 125 MHz, respectively, at the LeClaire-Dow Characterization Facility of the Department of Chemistry at the University of Minnesota. The solvent residual peak was used as the internal reference. Data for ^{1}H NMR as reported as follows: chemical shift (δ, ppm), multiplicity (s, singlet; d, doublet; t, triplet, m, multiplet), integration, coupling constants (Hz). Data for ^{13}C NMR are reported as chemical shifts (δ, ppm). Mass spectra (LR = low resolution, ESI MS = electrospray ionization mass spectrometry) were recorded on a Bruker BioTOF II at the Waters Center for Innovation in Mass Spectrometry of the Department of Chemistry at the

University of Minnesota. TEM images were collected on a JEOL JEM1210, FEI Tecnai T12, or on a JEOL 1200EXII at 120 kV. Relaxivities were measured at 37 °C and 1.5 T (60 MHz) on a Bruker Minispec mq60. The hydrodynamic size of the particles and aggregates was measured by dynamic light scattering (DLS) with a 90Plus/BI-MAS particle size analyzer (Brookhaven Instruments Corporation). Elemental analyses were performed by inductively coupled plasma optical emission spectroscopy (ICP OES) on a Thermo Scientific iCAP 6500 duo optical emission spectrometer by the Department of Geology at the University of Minnesota. Solid-state infrared spectra were recorded on a Thermo Nicolet 6700 FTIR using an ATR adapter. Data was collected between 700 and 3700 cm^{-1}. UV−vis spectra were measured with a Varian Cary 100 Bio Spectrophotometer at T = 20 °C. Data was collected between 200 and 800 nm using a quartz cell with a path length of 10 mm. Luminescence data were recorded on a Varian Eclipse Fluorescence spectrophotometer using a quartz cell with a path length of 10 mm, excitation slit width of 10 nm, emission slit width of 5 nm at T = 20 °C.

Relaxivity. Longitudinal (T_1) and transverse (T_2) relaxation times of the nanoparticles in mQ water were measured on a Bruker Minispec mq60 NMR Analyzer at 60 MHz and 37 °C according to the inverse recovery sequence and the Carr−Purcell−Meiboom−Gill sequence, respectively. The total concentration of iron of each sample was determined by the equation below. Briefly, 5 μL of each probe was suspended in 200 μL HNO_3 (aq) and 100 μL mQ water. Each sample was heated at 100 °C overnight, after which T_1 of each solution was measured. The resulting concentration of iron was calculated from a calibration plot obtained from standard solutions of $FeCl_3$ in 2:1 HNO_3:mQ water calibrated by ICP OES. For each probe, the longitudinal (r_1) and transverse (r_2) relaxivities were fitted to the following equation:

$$r_i[\mathrm{Fe}] = \frac{1}{T_{i,\mathrm{obs}}} - \frac{1}{T_{i,\mathrm{H_2O}}}, \quad \text{where} i = 1, 2$$

Fe_3O_4@oleic Acid. Oleic acid functionalized magnetite nanoparticles were synthesized according to the procedure reported by Sun et al.[42] Nanoparticles were characterized by TEM, DLS, powder XRD, and IR.

Dop-PEG-NH_2 (3). The amine terminated poly(ethylene glycol) was synthesized as previously reported.[41] Successful synthesis was established by ^{1}H NMR and LR ESI MS.

Fe_3O_4@Dop-PEG-NH_2 (4). The magnetite nanoparticles were refunctionalized with the catechol-terminated polymer (**3**) according to a biphasic procedure previously reported by our group.[19] Briefly, a dispersion of Fe_3O_4@oleic acid in hexane was stirred vigorously with a solution of the poly(ethylene glycol) (**3**) in mQ water:THF (2:1) at pH 14 for 2 h at 40 °C and 12 h at room temperature. The aqueous dispersion was filtered through a microfilterfuge (pore size = 0.6 μm) to remove any clustered nanoparticles. The filtrate was lyophilized, resuspended in mQ water, and stored at room temperature as an aqueous dispersion. Successful refunctionalization was established by IR (see Figure 3). Ligand exchange is facilitated by the significantly higher binding affinity of iron for catecholate versus carboxylate. This procedure advantageously minimizes aggregation during refunctionalization while maintaining the magnetism of the metallic core.[19]

DOTA-Phen (5). The macrocylic polyaminocarboxylate ligand was synthesized as previously reported.[20,25] Successful synthesis was established by ^{1}H NMR, ^{13}C NMR, and LR ESI MS.

Fe_3O_4@Dop-PEG-Eu-DOTAm-Phen (1). The macrocycle DOTA-Phen (**5**) (5.0 mg, 8.4 μmol) was dissolved in mQ water (1 mL). *N*,*N*′-Dicyclohexylcarbodiimide (DDC, 5.0 mg, 24 μmol) and *N*-hydroxysuccinimide (NHS, 3.0 mg, 26 μmol) were added to the reaction mixture. After stirring for 2 h at room temperature, an aqueous solution of Fe_3O_4@Dop-PEG-NH_2 (**4**, 200 μL, 8.6 mM_{Fe}, 1.7 μmol_{Fe}) and triethylamine (5 μL, 67 μmol) were added to the reaction mixture, which was stirred for an additional 7 h at room temperature. Following the addition of aqueous $EuCl_3$ (50 μL, 40 mM, 2.0 μmol), the pH of the reaction mixture was adjusted to 7 and further stirred at 40 °C for 60 h. The nanoparticles were filtered with a 10 kDa MW cutoff filter (Amicon) to remove any unreacted macrocycle and europium. The supernantant was resuspended in mQ water (1.0 mL) and filtered through a 10 kDa MW filter again. This last step was repeated thrice. The resulting nanoparticles were resuspended in mQ water. The resulting aqueous dispersion of **1** was stored at room temperature. Successful functionalization was assessed by IR and ICP OES. Elemental analysis (ICP-AES) indicated a ratio of Fe:Eu of 67:60.

Ru(bpy′)(phen)(dppz) (6). The ruthenium intercalator was synthesized as previously reported[26,43−45] with successful synthesis established by ^{1}H NMR, ^{13}C NMR, LR ESI MS, and UV−vis spectroscopy.

Fe_3O_4@Dop-PEG-Ru(bpy′)(phen)(dppz) (2). 1-Ethyl-3-(3-dimethylaminopropyl)carbodiimide (EDC, 1 mg, 6 μmol) and *N*-hydroxysuccinimide (NHS, 2 mg, 17 μmol) were added to an aqueous solution of the ruthenium complex Ru(bpy′)(phen)(dppz) (**6**, 1 mg, 0.5 μmol). The reaction mixture was stirred at room temperature for 1 h, after which an aqueous solution of **4** was added. The reaction mixture was further stirred at room temperature for 15 h. The nanoparticles were filtered with a 10 kDa MW cutoff filter (Amicon) to remove any unreacted macrocycle and europium. The supernantant was resuspended in mQ water (1.0 mL) and filtered through a 10 kDa MW filter again. This last step was repeated thrice. The resulting nanoparticles were resuspended in mQ water and filtered through a microfilterfuge (pore size 0.6 μm) to remove any aggregated nanoparticles. The resulting aqueous dispersion of **2** was stored at room temperature. Successful functionalization was assessed by IR and ICP OES. Elemental analysis indicated a ratio of Fe:Ru of 87:1.

AUTHOR INFORMATION

Corresponding Author

pierre@umn.edu

Notes

The authors declare no competing financial interest.

ACKNOWLEDGMENTS

This work was supported partially by the MRSEC Program of the National Science Foundation (DMR-0819885). Part of this work was carried out in the College of Science and Engineering Characterization Facility, University of Minnesota, which has received capital equipment funding from the NSF through the MRSEC, ERC, and MRI programs. E.D.S. gratefully acknowledges partial support from the NIH − Chemical Biology Interface Training Grant (GM 08700). We thank A. Massari and B. Jones for obtaining the IR spectra and K. Hurley for the TEM images.

REFERENCES

(1) Gandhi, S.; Venkatesh, S.; Sharma, U.; Jagannathan, N. R.; Sethuraman, S.; Krishnan, U. M. *J. Mater. Chem.* **2011**, *21*, 15698.

(2) Cha, E.-J.; Jang, E. S.; Sun, I.-C.; Lee, I. J.; Ko, J. H.; Kim, Y. I.; Kwon, I. C.; Kim, K.; Ahn, C.-H. *J. Controlled Release* **2011**, *155*, 152.

(3) Benyettou, F.; Lalatonne, Y.; Chebbi, I.; Benedetto, M. D.; Serfaty, J.-M.; Lecouvey, M.; Motte, L. *Phys. Chem. Chem. Phys.* **2011**, *13*, 10020.

(4) Kunzmann, A.; Andersson, B.; Thurnherr, T.; Krug, H.; Scheynius, A.; Fadeel, B. *Biochim. Biophys. Acta* **2011**, *1810*, 361.

(5) Kunzmann, A.; Andersson, B.; Vogt, C.; Feliu, N.; Ye, F.; Gabrielsson, S.; Toprak, M. S.; Buerki-Thurnherr, T.; Laurent, S.; Vahter, M.; Krug, H.; Muhammed, M.; Scheynius, A.; Fadeel, B. *Toxicol. Appl. Pharmacol.* **2011**, *253*, 81.

(6) Veiseh, O.; Sun, C.; Fang, C.; Bhattarai, N.; Gunn, J.; Kievit, F.; Du, K.; Pullar, B.; Lee, D.; Ellenbogen, R. G.; Olson, J.; Zhang, M. *Cancer Res.* **2009**, *69*, 6200.

(7) Wan, S.; Huang, J.; Guo, M.; Zhang, H.; Cao, Y.; Yan, H.; Liu, K. *J. Biomed. Mater. Res., Part A* **2007**, *80A*, 946.

(8) Kell, A. J.; Barnes, M. L.; Jakubek, Z. J.; Simard, B. *J. Phys. Chem. C* **2011**, *115*, 18412.
(9) Smolensky, E. D.; Neary, M. C.; Zhou, Y.; Berquo, T. S.; Pierre, V. C. *Chem. Commun.* **2011**, *47*, 2149.
(10) Leung, K. C. F.; Xuan, S. H.; Zhu, X. M.; Wang, D. W.; Chak, C. P.; Lee, S. F.; Ho, W. K. W.; Chung, B. C. T. *Chem. Soc. Rev.* **2012**, *41*, 1911.
(11) Xi, P. X.; Cheng, K.; Sun, X. L.; Zeng, Z. Z.; Sun, S. H. *J. Mater. Chem.* **2011**, *21*, 11464.
(12) Li, M.-J.; Chen, Z.; Yam, V. W.-W.; Zu, Y. *ACS Nano* **2008**, *2*, 905.
(13) Zhang, L. H.; Liu, B. F.; Dong, S. J. *J. Phys. Chem. B* **2007**, *111*, 10448.
(14) Hou, J. G.; Gan, N.; Hu, F. T.; Zheng, L.; Cao, Y. T.; Li, T. H. *Int. J. Electrochem. Sci.* **2011**, *6*, 2845.
(15) Smolensky, E. D.; Zhou, Y.; Pierre, V. C. *Eur. J. Inorg. Chem.* **2012**, 2141.
(16) Xi, P. X.; Cheng, K.; Sun, X. L.; Zeng, Z. Z.; Sun, S. H. *Chem. Commun.* **2012**, *48*, 2952.
(17) Kell, A. J.; Barnes, M. L.; Jakubek, Z. J.; Simard, B. *J. Phys. Chem. C* **2011**, *115*, 18412.
(18) Weitz, E. A.; Lewandowski, C.; Smolensky, E. D.; Marjanska, M.; Pierre, V. C. submitted for publication.
(19) Smolensky, E. D.; Park, H.-Y. E.; Berquó, T. S.; Pierre, V. C. *Contrast Media Mol. Imaging* **2011**, *6*, 189.
(20) Weitz, E. A.; Chang, J. Y.; Rosenfield, A. H.; Pierre, V. C. *J. Am. Chem. Soc.* **2012**, *134*, 16099.
(21) Bobba, G.; Dickins, R. S.; Kean, S. D.; Mathieu, C. E.; Parker, D.; Peacock, R. D.; Siligardi, G.; Smith, M. J.; Gareth Williams, J. A.; Geraldes, C. F. G. C. *J. Chem. Soc., Perkin Trans. 2* **2001**, 1729.
(22) Bobba, G.; Kean, S. D.; Parker, D.; Beeby, A.; Baker, G. *J. Chem. Soc., Perkin Trans. 2* **2001**, 1738.
(23) Bobba, G.; Frias, J. C.; Parker, D. *Chem. Commun.* **2002**, 890.
(24) Bobba, G.; Bretonniere, Y.; Frias, J. C.; Parker, D. *Org. Biomol. Chem.* **2003**, *1*, 1870.
(25) Weitz, E. A.; Chang, J. Y.; Rosenfield, A. H.; Morrow, E. A.; Pierre, V. C. submitted for publication.
(26) Friedman, A. E.; Chambron, J. C.; Sauvage, J. P.; Turro, N. J.; Barton, J. K. *J. Am. Chem. Soc.* **1990**, *112*, 4960.
(27) Friedman, A. E.; Kumar, C. V.; Turro, N. J.; Barton, J. K. *Nucleic Acids Res.* **1991**, *19*, 2595.
(28) Hartshorn, R. M.; Barton, J. K. *J. Am. Chem. Soc.* **1992**, *114*, 5919.
(29) Jenkins, Y.; Friedman, A. E.; Turro, N. J.; Barton, J. K. *Biochemistry* **1992**, *31*, 10809.
(30) Dupureur, C. M.; Barton, J. K. *Inorg. Chem.* **1997**, *36*, 33.
(31) Olson, E. J. C.; Hu, D.; Hormann, A.; Jonkman, A. M.; Arkin, M. R.; Stemp, E. D. A.; Barton, J. K.; Barbara, P. F. *J. Am. Chem. Soc.* **1997**, *119*, 11458.
(32) Holmlin, R. E.; Stemp, E. D. A.; Barton, J. K. *Inorg. Chem.* **1998**, *37*, 29.
(33) Lim, M. H.; Song, H.; Olmon, E. D.; Dervan, E. E.; Barton, J. K. *Inorg. Chem.* **2009**, *48*, 5392.
(34) Song, H.; Kaiser, J. T.; Barton, J. K. *Nat. Chem.* **2012**, *4*, 615.
(35) Bogdanov, A., Jr.; Matuszewski, L.; Bremer, C.; Petrovsky, A.; Weissleder, R. *Mol. imaging* **2002**, *1*, 16.
(36) Josephson, L.; Perez, J. M.; Weissleder, R. *Angew. Chem., Int. Ed. Engl.* **2001**, *40*, 3204.
(37) Perez, J. M.; Josephson, L.; O'Loughlin, T.; Hogemann, D.; Weissleder, R. *Nat. Biotechnol.* **2002**, *20*, 816.
(38) Perez, J. M.; O'Loughin, T.; Simeone, F. J.; Weissleder, R.; Josephson, L. *J. Am. Chem. Soc.* **2002**, *124*, 2856.
(39) Perez, J. M.; Simeone, F. J.; Saeki, Y.; Josephson, L.; Weissleder, R. *J. Am. Chem. Soc.* **2003**, *125*, 10192.
(40) Zhao, M.; Josephson, L.; Tang, Y.; Weissleder, R. *Angew. Chem., Int. Ed. Engl.* **2003**, *42*, 1375.
(41) Smolensky, E. D.; Marjanska, M.; Pierre, V. C. *J. Chem. Soc., Dalton Trans.* **2012**, *41*, 8039.
(42) Sun, S.; Zeng, H.; Robinson, D. B.; Raoux, S.; Rice, P. M.; Wang, S. X.; Li, G. *J. Am. Chem. Soc.* **2003**, *126*, 273.
(43) Sitlani, A.; Long, E. C.; Pyle, A. M.; Barton, J. K. *J. Am. Chem. Soc.* **1992**, *114*, 2303.
(44) Holmlin, R. E.; Yao, J. A.; Barton, J. K. *Inorg. Chem.* **1999**, *38*, 174.
(45) Holmlin, R. E.; Dandliker, P. J.; Barton, J. K. *Bioconjugate Chem.* **1999**, *10*, 1122.
(46) Smolensky, E. D.; Park, H.-Y. E.; Zhou, Y.; Rolla, G. A.; Marjanska, M.; Botta, M.; Pierre, V. C. *J. Mat. Chem. B* **2013**, *1*, 2818–2828.
(47) Roch, A.; Gillis, P.; Ouakssim, A.; Muller, R. N. *J. Magn. Magn. Mater.* **1999**, *201*, 77.
(48) Roch, A.; Muller, R. N.; Gillis, P. *J. Chem. Phys.* **1999**, *110*, 5403.